STScI | SPACE TELESCOPE SCIENCE INSTITUTE

JWST TECHNICAL REPORT

Title: NIRISS Commissioning Results: NIS-011(b) – NIRISS Geometric Distortion Calibration (NGAS CAR-374, APT 1086)	Doc #: JWST-STScI-008323, SM-12 Date: 5 December 2022 Rev: -
Authors: S. Tony Sohn and the NIRISS team Phone: 410 – 338 - 6763	Release Date: 4 January 2023

1 Abstract

This report summarizes the analysis and results of the commissioning program NIS-011b (NGAS CAR-374, APT 1086). We describe the data and the analysis used for calibrating the geometric distortion of NIRISS from this commissioning program. We analyzed a total of 216 individual NIRISS images (12 filters × 18 dithers) obtained through program 1086 using a python script specifically written for distortion calibrations. Stars detected in our NIRISS images were crossmatched with an astrometric catalog based on HST astrometry. For each image in each filter, we fit a 5th-order polynomial to the crossmatched positions to derive distortion solutions. We then averaged 18 individual distortion results for each filter. We find systematic residual patterns across all filters. However, the resulting solutions have rms of <0.7 mas per axis, far lower than the mission requirement of 5 mas. The SIAF distortion has been updated using the F150W distortion coefficients, and the distortion reference files for all NIRISS filters have been delivered to CRDS.

2 Description of Data

For our NIRISS geometric distortion calibration program, we targeted fields within the LMC Calibration Field characterized by a 5′ × 5′ HST-based catalog, tied into the reference frame defined by the Gaia DR2 positions with median astrometric uncertainties of 0.26 mas (Anderson et al. 2021). Observations were taken in all 12 filters available for NIRISS imaging. For each filter, there were 18 individual images obtained in a 3×3 mosaic pointing with 75% overlap in rows and columns. The data files and exposure specifications are listed in Table 1.

Table 1. Properties of exposures from APT program 1086 used for the distortion calibration analysis. The first three columns provide numbers for FITS file root names in the form jw01086001<vvv>_<gg>101_0000<e>_nis where <vvv> is the visit number, <gg> is the visit group, and <e> is the exposure/dither number.

vvv	gg	e	Pupil	Filter	Readout Pattern	N_{GROUPS}	N_{INTS}	T_{EXP} (s)
001 002, 003 004	14, 38, 62, 86 14, 38 14	1, 2 1, 2 1, 2	CLEAR	F090W	NISRAPID	5	1	128.84
001 002, 003 004	16, 40, 64, 88 16, 40 16	1, 2 1, 2 1, 2	CLEAR	F115W	NISRAPID	5	1	128.84
001	20, 44, 68, 92	1, 2	CLEAR	F140M	NISRAPID	5	1	128.84

vvv	gg	e	Pupil	Filter	Readout Pattern	NGROUPS	NINTS	TEXP (s)
002, 003 004	20, 44 20	1, 2 1, 2						
001 002, 003 004	22, 46, 70, 94 22, 46 22	1, 2 1, 2 1, 2	CLEAR	F150W	NISRAPID	5	1	128.84
001 002, 003 004	18, 42, 66, 90 18, 42 18	1, 2 1, 2 1, 2	CLEAR	F158M	NISRAPID	5	1	128.84
001 002, 003 004	24, 48, 72, 96 24, 48 24	1, 2 1, 2 1, 2	CLEAR	F200W	NISRAPID	5	1	128.84
001 002, 003 004	02, 26, 50, 74 02, 26 02	1, 2 1, 2 1, 2	F277W	CLEARP	NISRAPID	10	1	236.21
001 002, 003 004	06, 30, 54, 78 06, 30 06	1, 2 1, 2 1, 2	F356W	CLEARP	NISRAPID	10	1	236.21
001 002, 003 004	10, 34, 58, 82 10, 34 10	1, 2 1, 2 1, 2	F380M	CLEARP	NISRAPID	15	1	343.58
001 002, 003 004	08, 32, 56, 80 08, 32 08	1, 2 1, 2 1, 2	F430M	CLEARP	NISRAPID	15	1	343.58
001 002, 003 004	04, 28, 52, 76 04, 28 04	1, 2 1, 2 1, 2	F444W	CLEARP	NISRAPID	10	1	236.21
001 002, 003 004	12, 36, 60, 84 12, 36 12	1, 2 1, 2 1, 2	F480M	CLEARP	NISRAPID	15	1	343.58

3 Analysis

Initial distortion solutions for NIRISS have been modeled with Code V by Honeywell (Martel & Fullerton 2016). NIS-011b program was designed to measure the on-orbit distortion solutions and update the coefficients as necessary for the first time after the JWST launch. For the distortion calibration analysis, we used the python script `jwst_distortion.py` which is part of the `jwst_fpa` package (see the github webpage https://github.com/tonysohn/jwst_fpa for more details). The original version of this script was introduced in Sahlmann (2019). `jwst_distortion.py` performs the following steps:

- Extract sources and measure position of stars in the observed NIRISS images.
- Crossmatch stars from the images to calibration catalog stars.
- Use bivariate polynomials of degree $\geqq 4$ to map the measured positions of stars to the catalog positions.
- Zero-point offsets with respect to the V-frame origin (boresight) and orientation of the detector Y-axis against telescope V3-axis are forced to be zero since those are calibrated in a separate program (NIS-13).
- Convert polynomial coefficients derived from above to formats consistent with the SIAF products and the distortion reference files.

Details of these steps are described below. For the sake of brevity, we provide diagnostic plots for only one example case of F150W image (*jw01086001001_22101_00001_cal.fits*).

3.1 Source detection and astrometry

The `jwst_distortion.py` script starts with the source detection stage running the *IRAFStarFinder* module from the *photutils* python package (Bradley et al. 2019) on _cal.fits image files. The pixel values of _cal.fits images are first divided by `PHOTMJSR` (flux density producing 1 count per second or cps) found in the FITS header to convert the units of each pixel values to cps. For the source detection, we selected a set of parameters that work best for images obtained with each filter. This was done by testing different parameter sets in *IRAFStarFinder* outside of the script and visually inspecting the detection results. The goal here was to detect as many stars as possible while avoiding spurious detections. The FWHMs of stars varied across different filters, so for the convolution of Gaussian kernels, we decided to use filter-dependent FWHMs as listed in Table 2. As for the sharpness and roundness parameters, we used $0.7 < \text{sharpness} < 1.3$ and $0.0 < \text{round} < 0.4$ consistently for all images. All sources that satisfy these conditions that are 3-σ above the background were initially accepted as stars. We then applied additional filtering based on the measured flux, i.e., any source with flux lower than an absolute total count of 50 cps (poor positional measurements), and higher than the top 99.5% percentile (mostly saturated sources) were filtered out.

Table 2. FWHM used for each filter in the source detection stage via *IRAFStarFinder*.

Filters	FWHM (pixel)
F090W, F115W	1.4
F140M, F150W, F158M, F200W, F277W	1.5
F356W	1.6
F380M	1.7
F430M, F444W, F480M	1.8

Positions of sources were determined using the `centroid_2dg` algorithm to mitigate pixel-phase issues for undersampled PSFs following Goudfrooij (2022). Figure 1 shows an example F150W image used in our calibration. We also show the centroid positions of the calibration stars as selected from the method described above in blue circles.

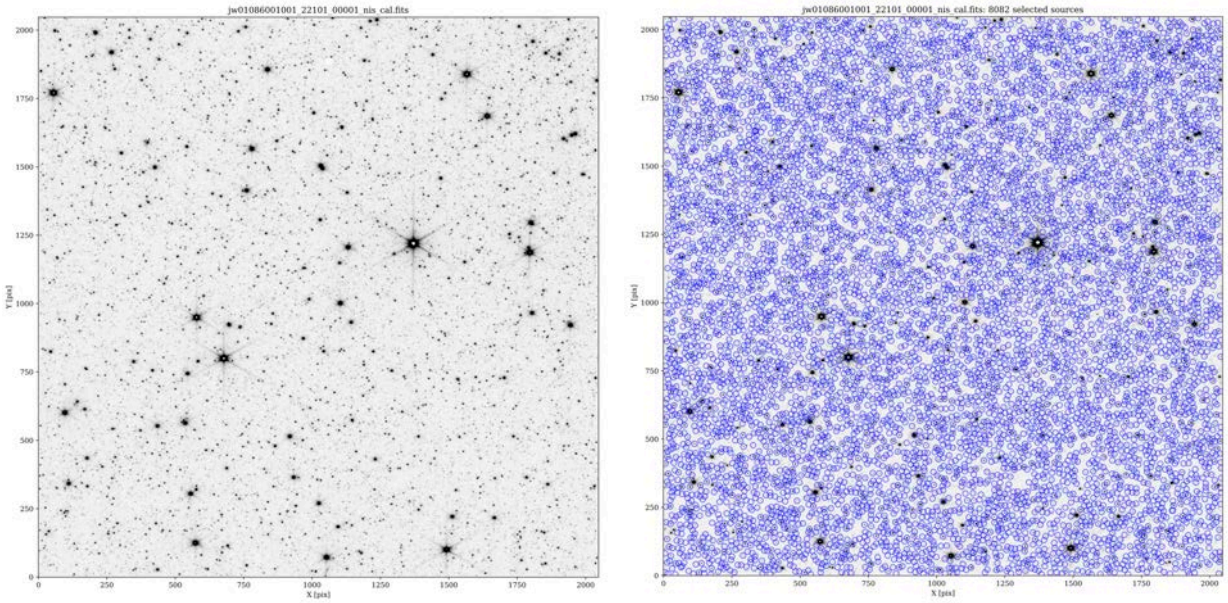

Figure 1. (Left) One of the F150W images (jw01086001001_22101_00001_cal.fits) used for the distortion calibration. (Right) Same image as the left but all sources used for the distortion calibration circled in blue.

3.2 Crossmatching with reference catalog

Next step is to crossmatch the measured stars with the astrometric reference catalog. To do this, the script first transforms (RA, Dec) positions of the reference catalog to the telescope (V2, V3) coordinates using the pointing information (RA_V1, DEC_V1, PA_V3) commanded during the observations via *pysiaf*. The positions of detected sources are also transformed to the telescope coordinates using the operational (in this case, ground-determined) SIAF alignment parameters + distortion coefficients via *pysiaf*. Once the two sets of catalogs are projected onto the telescope coordinates, crossmatching is performed in a two-step process: first, a global offset in (V2, V3) is computed and applied based on up to 200 brightest stars detected using the `matchutils` module in the `tweakwcs` package; second, a nearest-neighbor match is performed using a match radius of 0.3 arcsec (equivalent to ~4.5 NIRISS pixels). The crossmatching employed an iterative 4-σ outlier rejection to minimize false matches. Results of crossmatching for the example case are shown in Figure 2.

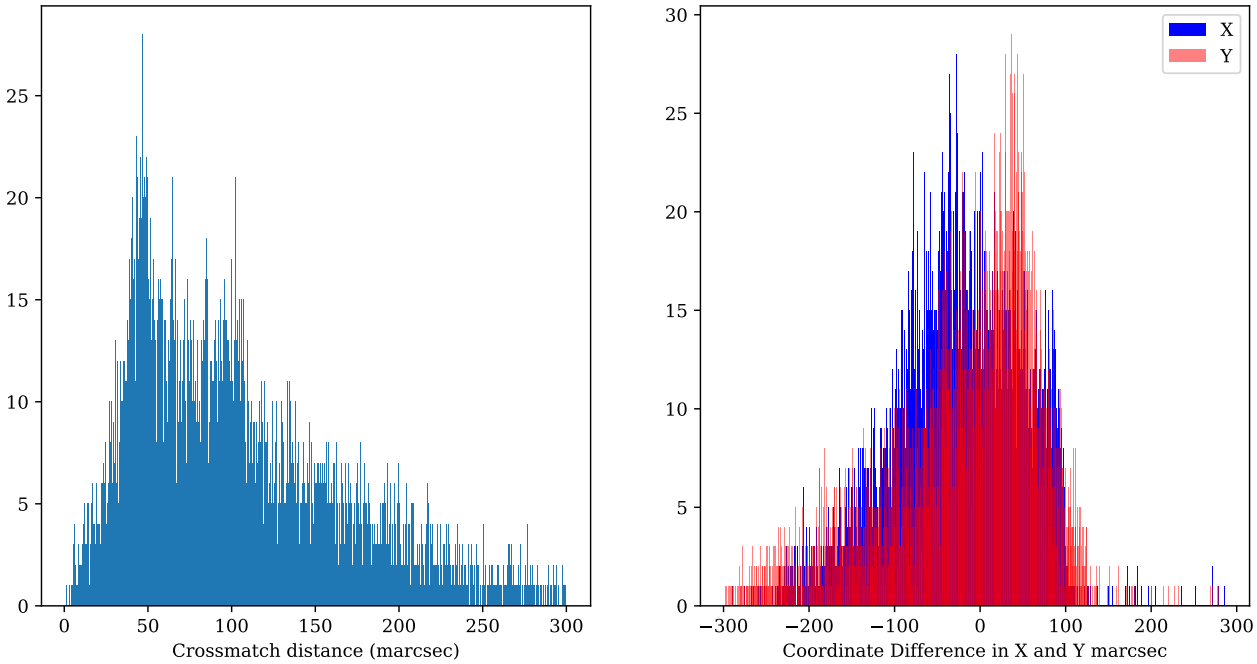

Figure 2. Histograms of crossmatching distance (left) and X, Y residuals (right) in milliarcseconds for the example case of jw01086001001_22101_00001_cal.fits. Ordinates for both plots represent number of sources.

3.3 Deriving the distortion polynomial coefficients

Using the crossmatched catalog, the script solves a 2-dimensional polynomial for the distortion calibration. Following the standard distortion model described in Cox & Lallo (2017), the forward distortion solution (*sci* → *idl*) is expressed as

$$Xidl = \sum_{i=1}^{deg} \sum_{j=0}^{i} A_{i,j} \, (Xsci - XsciRef)^{i-j} \, (Ysci - YsciRef)^{j}$$

$$Yidl = \sum_{i=1}^{deg} \sum_{j=0}^{i} B_{i,j} \, (Xsci - XsciRef)^{i-j} \, (Ysci - YsciRef)^{j}$$

where the input (*Xsci, Ysci*) positions are directly taken from the centroids in the previous steps, corresponding ideal coordinates (*Xidl*, *Yidl*) are transformed from the (V2, V3) coordinates of the crossmatched reference catalog using the operational SIAF parameters, and (*XsciRef*, *YsciRef*) indicate the reference *sci* pixel coordinates – for the NIRISS detectors, we adopt (*XsciRef*, *YsciRef*) = (1024.5, 1024.5) since all of our distortion solutions are based on the NIS_CEN parent aperture. The script solves for $A_{i,j}$ and $B_{i,j}$ given the inputs through an iterative process until convergence. For each iteration, a 2.5-σ outlier rejection is applied to ensure reliability in the solutions.

3.4 Order of polynomial solutions

The default NIRISS geometric distortion in the operational SIAF is represented by a 4th-order polynomial (i.e., *deg*=4 in the equations above). However, while analyzing the NIS-011 commissioning data using a 4th-order polynomial, we found unexpected systematic trends in the fit residuals: the Δx vs. x and Δy vs. y (where Δ refers to the residuals, i.e., measured minus expected positions) exhibit non-negligible sinusoidal or 'wavy' patterns with peak-to-peak values reaching up to ~15 mas. These trends with similar degrees and shapes were observed in polynomial residuals for all filters which implies that the cause is likely of detector origin but not filter-dependent. We tested whether increasing the polynomial order of distortion solutions reduces the systematic trends and Figure 3 represents the results. The polynomial orders start from 2 and goes up to 7 in this figure to illustrate how increasing them progressively reduces large-scale systematics. Overall, the residuals are improved with the increase of orders as expected, but we find a pronounced improvement when increasing the order from 4 to 5. Beyond that, there is only a minimal improvement. In principle, higher-order polynomials will fit the data better than lower-orders, but there is always the danger of overfitting especially near the edges of detector in our case. We therefore decided to adopt a polynomial order of 5 for NIRISS, i.e., the same order as NIRCam.

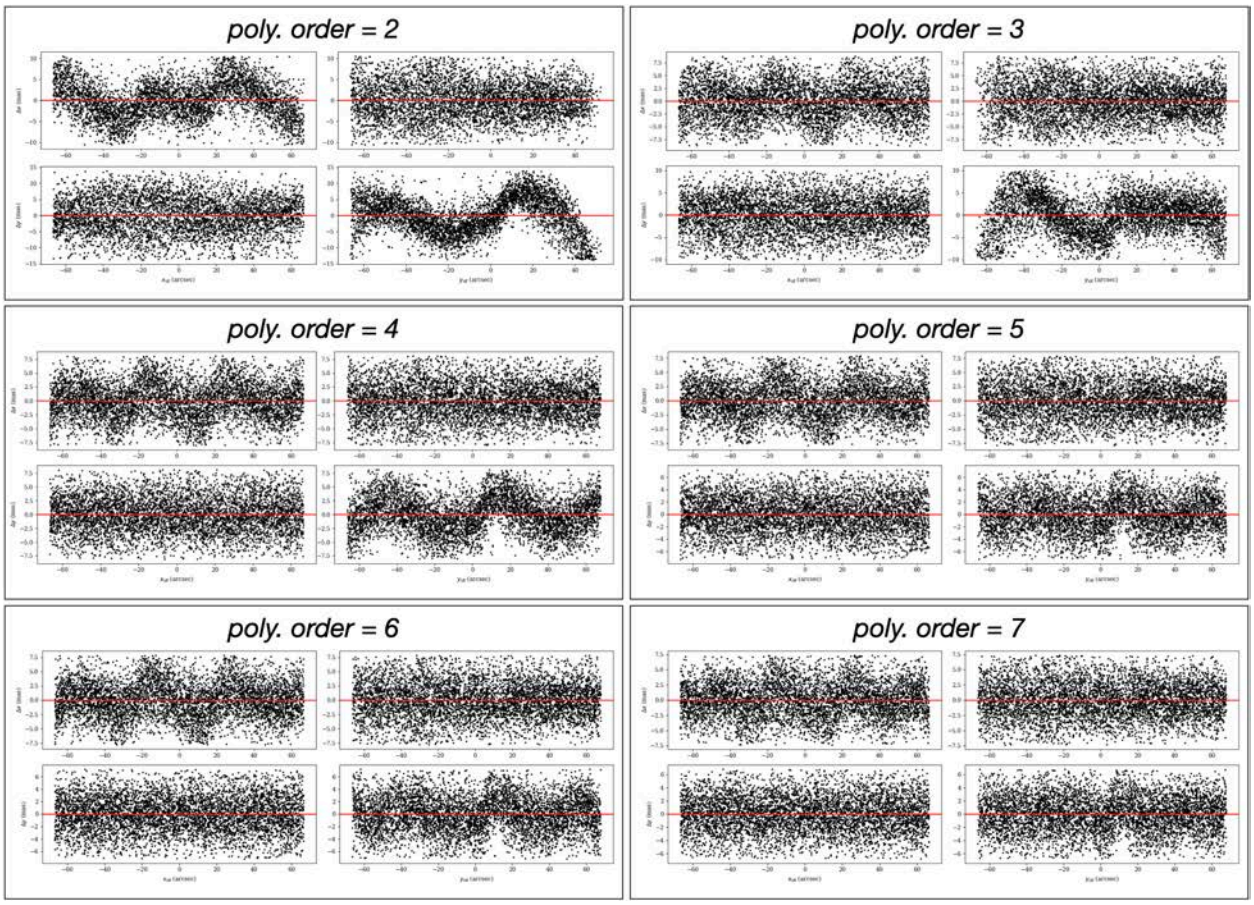

Figure 3. Residuals of the polynomial solutions as a function of 1-D spatial coordinates for orders 2 to 7. For each polynomial order, the following residuals are plotted: Δx vs. x (top left); Δx vs. y (top right); Δy vs. x (bottom left); Δy vs. y (bottom right). Note that the ordinates do not always show same range.

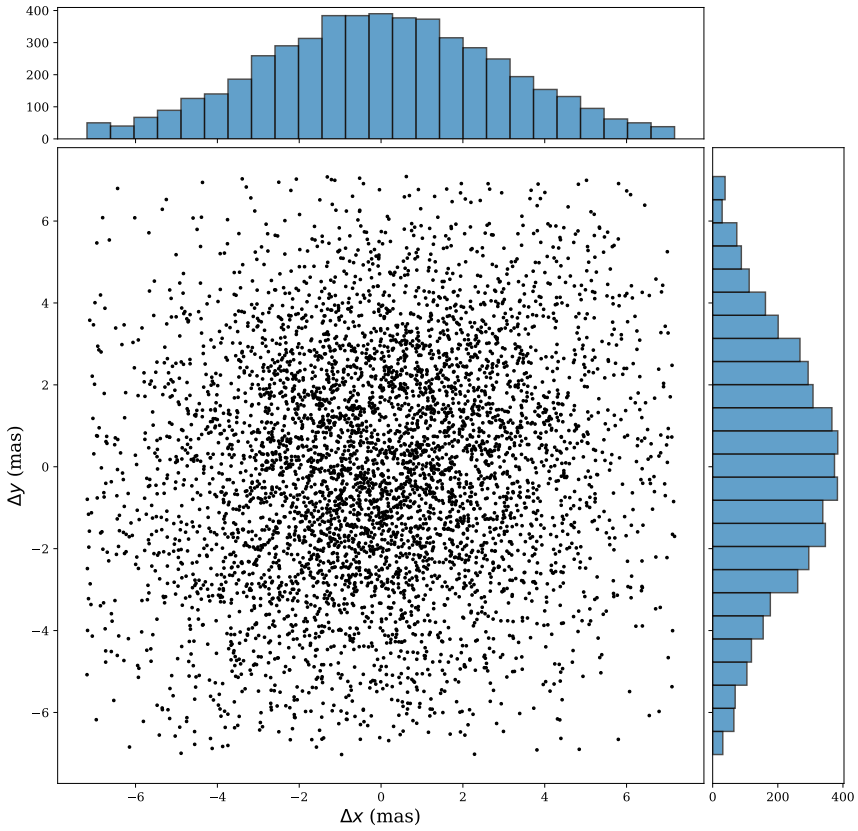

Figure 4. Residuals of the polynomial distortion solution in Y vs. X for a single F150W calibration data (jw01086001001_22101_00001_cal.fits).

3.5 Removing global offset and Y-rotation terms in polynomial coefficients

The polynomial solutions derived as described above include non-zero global offset and Y-rotation terms resulting from uncertainties in telescope pointing during observations and SIAF alignments (i.e., precise location and position angle of the detector in the focal plane). Based on the SIAF convention (Cox & Lallo 2017), the distortion solutions should be independent from these uncertainties and have the relevant terms set to zero. To do this, we subtracted the global offsets and applied the rotation to the polynomial coefficients such that the A_{00}, B_{00}, and A_{11} terms in the equations above become zero. We note that the uncertainties in pointing and SIAF alignments are handled separately in the NIS-13 calibration (Sohn et al. 2022), and the distortion coefficients are independent from these by definition as they only relate to positions within the detector.

3.6 Residuals and final solutions

The Δx and Δy residuals after fitting a 5th-order polynomial for the example case are shown in Figure 4. Despite the remaining systematic residuals as seen in Figure 3, the rms of solution for this single case is only 2.8 mas per axis which is already below the requirement of 5 mas. For each filter, we analyzed 18 images separately and derived 18 independent distortion solutions. We then averaged each coefficient from these 18 solutions, hence providing a robust determination of the

distortion coefficients. The resulting rms of solutions for all filters along with the number of stars per exposure used for the distortion calibration are presented in Table 3.

Table 3. Number of stars used per exposure and rms of distortion solutions for each filter.

Filter	Nstars per exp.	rms (mas)	Filter	Nstars per exp.	rms (mas)
F090W	~6,700	0.65	F277W	~4,000	0.59
F115W	~6,100	0.66	F356W	~2,700	0.59
F140M	~5,600	0.67	F380M	~900	0.56
F150W	~6,000	0.66	F430M	~800	0.57
F158M	~5,500	0.62	F444W	~1,700	0.59
F200W	~4,000	0.59	F480M	~700	0.57

3.7 Comparison against ground-determined (previous) distortion solutions

Figure 6 illustrates the newly-derived distortion solution for the F150W filter compared against the ground-determined one as vectors originating from regular grid points. This plot was generated as follows. We first define a regular set of 25×25 grid points in the (*Xsci*, *Ysci*) coordinate frame. These grid points are transformed into (*Xidl*, *Yidl*) coordinate frame using (1) the ground-defined polynomial coefficients and (2) the new coefficients. Then we calculate the vector corresponding to (2)−(1) for each grid point and plot these in arrows with normalized length.

The overall pattern in Figure 5 implies that there is a global scale difference between the old and new distortion properties. The same trend is seen across all filters, and also for the other detectors as found during the OTE commissioning stage. This is likely due to the slight change in focal length of the telescope before and after the JWST launch. In addition to the scale change, there is also a hint of asymmetric vector distribution which may indicate a slight tilt of the NIRISS detector, although it is difficult to judge by just inspecting the distortion properties.

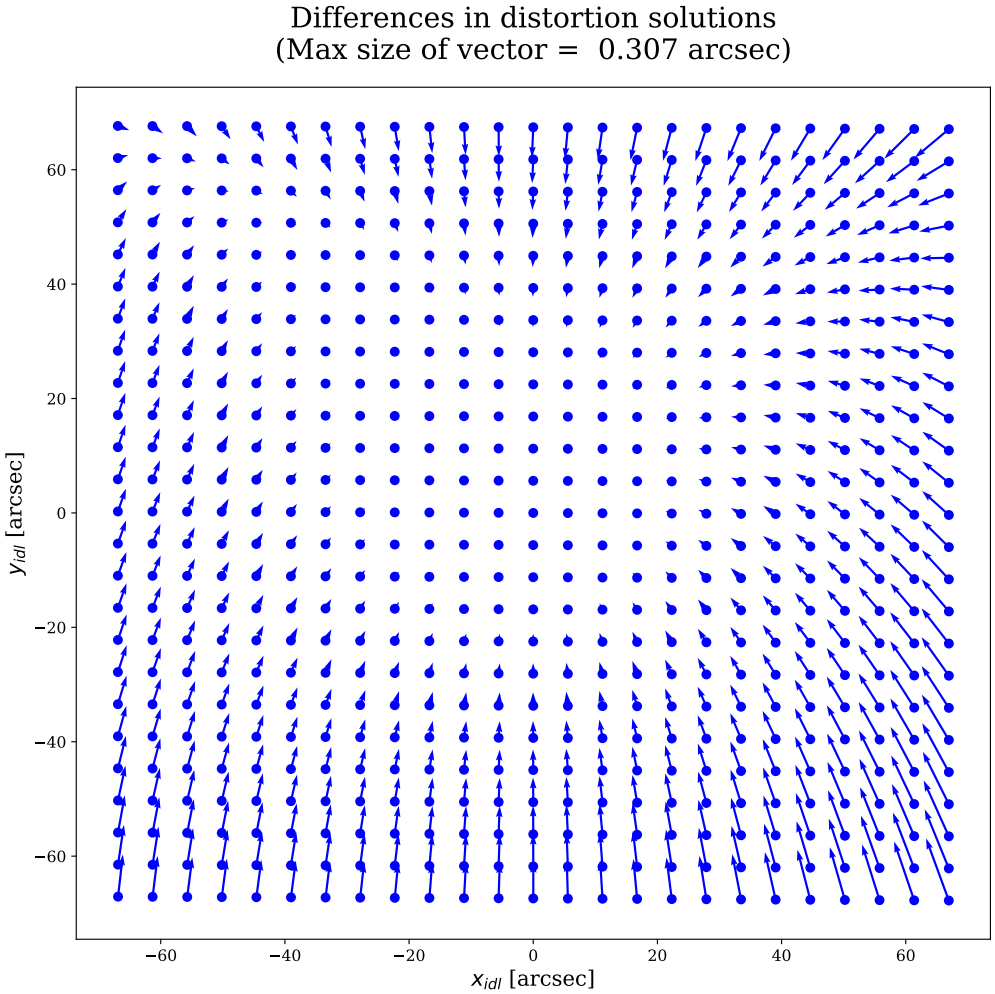

Figure 5. Comparison between the new F150W distortion solution derived in this program and the ground-determined one.

3.8 Inverse distortion polynomial coefficients

Both the SIAF and reference files require not only the forward (*sci→idl*) distortion coefficients but also the inverse (*idl→sci*) distortion coefficients. The inverse distortion solution takes the following form:

$$Xsci - XsciRef = \sum_{i=1}^{deg} \sum_{j=0}^{i} C_{i,j}\, Xidl^{i-j}\, Yidl^{j}$$

$$Ysci - YsciRef = \sum_{i=1}^{deg} \sum_{j=0}^{i} D_{i,j}\, Xidl^{i-j}\, Yidl^{j}$$

To derive $C_{i,j}$ and $D_{i,j}$ coefficients from the equations above, we used the same procedure as for the forward solutions but with the roles of the observed and crossmatched reference catalog positions reversed. The averaging of each coefficient was done in similar fashion.

3.9 Distortion calibration products

There are two types of products resulting from this calibration program:

(1) An ASCII text file which gets incorporated into the SIAF xml file along with the SIAF alignment parameters (see Sohn 2022 for details) – for this we use the F150W filter result, the same filter used for SIAF alignment calibration. The SIAF xml file gets delivered to the Project Reference Database (PRD) for various operational tasks related to telescope pointing, guiding, target acquisitions, and etc. The content of the ASCII file named `niriss_siaf_distortion_nis_cen.txt` is shown in Figure 6. Columns *Sci2IdlX* and *Sci2IdlY* correspond to A_{ij} and B_{ij} in equations above, respectively. Similarly, *Idl2SciX* and *Idl2SciY* correspond to C_{ij} and D_{ij}.

```
# NIRISS distortion coefficient file

# Aperture: NIS_CEN
# Filter/Pupil: CLEAR/F150W
# Generated 2022-05-05T23:20:14.199 utc
# by tsohn
#
AperName , siaf_index , exponent_x , exponent_y ,          Sci2IdlX ,          Sci2IdlY ,          Idl2SciX ,          Idl2SciY
 NIS_CEN ,          0 ,          0 ,          0 ,               0.0 ,               0.0 ,               0.0 ,               0.0
 NIS_CEN ,         10 ,          1 ,          0 ,     0.065324254028 , -0.00029946015481 ,      15.308186136 ,     0.069871045863
 NIS_CEN ,         11 ,          0 ,          1 ,  1.5058363507e-21 ,     0.065814937584 , -9.6373526443e-19 ,      15.194589313
 NIS_CEN ,         20 ,          2 ,          0 , -1.7083833429e-08 ,  5.6197596354e-08 ,  6.0862031033e-05 , -0.00020018307403
 NIS_CEN ,         21 ,          1 ,          1 ,  1.1016773619e-08 , -3.2584152155e-08 , -4.0078904507e-05 ,  0.00011208181103
 NIS_CEN ,         22 ,          0 ,          2 , -7.5599856304e-10 ,   6.826992809e-08 ,  2.2647272728e-06 , -0.00025313897788
 NIS_CEN ,         30 ,          3 ,          0 , -1.2608447518e-11 ,  1.5070637916e-12 ,  6.9612559913e-07 ,  -7.858306482e-08
 NIS_CEN ,         31 ,          2 ,          1 , -9.0572145968e-12 , -1.6269513768e-11 ,  4.9554508445e-07 ,  8.5820259707e-07
 NIS_CEN ,         32 ,          1 ,          2 , -9.5108876015e-12 , -7.9191549007e-12 ,  4.7519407648e-07 ,  5.0115960286e-07
 NIS_CEN ,         33 ,          0 ,          3 , -4.7544601824e-12 , -1.0222646202e-10 ,  2.5190498134e-07 ,  5.3638177941e-06
 NIS_CEN ,         40 ,          4 ,          0 , -2.8253423495e-15 , -3.8458837089e-16 ,   2.427562465e-09 ,  3.2035274246e-10
 NIS_CEN ,         41 ,          3 ,          1 ,  2.4379566319e-15 , -2.3037891845e-15 ,  -2.315823743e-09 ,  2.1850794198e-09
 NIS_CEN ,         42 ,          2 ,          2 ,  -3.015054153e-15 , -2.7188225555e-14 ,  2.9566842675e-09 ,  2.2369575581e-08
 NIS_CEN ,         43 ,          1 ,          3 , -2.0586547132e-14 ,  1.1871491244e-14 ,   1.718217979e-08 , -9.1218254834e-09
 NIS_CEN ,         44 ,          0 ,          4 ,  9.6282229723e-16 , -3.9661526791e-14 , -7.4629620756e-10 ,   3.424164376e-08
 NIS_CEN ,         50 ,          5 ,          0 ,  1.0134370635e-18 , -1.6609420259e-18 , -1.3034795395e-11 ,  2.0801892117e-11
 NIS_CEN ,         51 ,          4 ,          1 ,   2.602901056e-18 ,  2.6238531415e-20 , -3.2508796989e-11 , -9.8589251849e-13
 NIS_CEN ,         52 ,          3 ,          2 , -1.3938501382e-17 ,  5.9235720614e-18 ,  1.7616598724e-10 , -7.3333411101e-11
 NIS_CEN ,         53 ,          2 ,          3 ,  9.5536213663e-18 ,  2.4140733771e-18 , -1.2033769504e-10 , -3.3103369497e-11
 NIS_CEN ,         54 ,          1 ,          4 ,  4.4471618224e-18 , -1.2344473054e-18 ,  -5.602156015e-11 ,  8.3465598497e-12
 NIS_CEN ,         55 ,          0 ,          5 ,  1.1008926172e-18 ,  3.9769800618e-17 , -1.3183850335e-11 , -4.9212971279e-10
```

Figure 6. Content of `niriss_siaf_distortion_nis_cen.txt` file

(2) Seperate reference files in *asdf* format for 12 NIRISS filters that are used by the *jwst* pipeline. For the reference files generation, we used a python tool that converts the ASCII text-style file in (1) to the standard *asdf* distortion reference file format. Distortion reference files have been delivered to the CRDS on May 18, 2022.

3.10 Systematic residuals and mitigation strategies

Our NIRISS distortion results from NIS-011 still exhibits unexplained 'wavy' systematic residuals (see Figure 3). Since the rms of the residual is well below the mission requirements, this has negligible impact on SIAF-related issues such as observation planning through APT, telescope

pointing, and target acquisition. However, the remaining systematics will have negative effect for science programs requiring high-precision astrometry. We have already shown that the residuals cannot be mitigated through simply increasing the polynomial orders implying that non-linear (or even spatially periodic) corrections are necessary. Indeed, our preliminary investigation shows that adopting a look-up table style correction in addition to the distortion polynomials, similar to how distortion corrections are done for HST ACS/WFC and WFC3/UVIS, will improve the distortion residuals significantly. Such corrections will not be possible for SIAF distortions under current schemes, but it is certainly possible to implement in the JWST calibration pipeline through distortion reference files in the future.

4 Acknowledgements

We would like to thank Armin Rest for providing python routines that allowed combining the polynomial coefficients from multiple measurements in an efficient manner. We would also like to thank Mattia Libralato for the independent verification of our results and the discussion about using look-up table corrections.

5 References

Anderson, J., Fall, M., and the Astrometry Working Group, 2021, "The JWST Calibration Field: Absolute Astrometry and Proper Motions with GAIA and a Second HST Epoch", JWST Technical Report JWST-STScI-007716, SM-12

Bradley, L., Sipocz, B. Robitaille, T., et al., 2022, astropy/photutils:v1.4.0, https://doi.org/10.5281/zenodo.6385735

Cox, C., & Lallo, M., 2017, "Description and Use of the JWST Science Instrument Aperture File", JWST Technical Report JWST-STScI-001550, SM-12

Goudfrooij, P., 2022, "Accuracy and Precision of Centroid Algorithms in the `photutils` Python package for NIRISS Point Spread Functions", JWST Technical Report JWST-STScI-008116, SM-12

Martel, A., & Fullerton, A., 2016, "The Geometric Distortion of NIRISS", JWST Technical Report JWST-STScI-003524, SM-12

Sahlmann, J., 2017, "Astrometric Accuracy of the JWST Calibration Field Catalog examined with the first Gaia Data Release", JWST Technical Report JWST-STScI-005492, SM-12

Sahlmann, J., 2019, "Distortion Calibration of JWST Imagers: End-to-end Simulation for NIRISS", JWST Technical Report JWST-STScI-007075, SM-12

Sohn, S. T., et al., 2022, "NIRISS Commissioning Results: NIS-013(a) – NIRISS-FGS Alignment and SIAF Update (NGAS CAR-376, APT 1088)", JWST Technical Report, in preparation